Available online at www.sciencedirect.com
ScienceDirect
Journal of Sound and Vibration 303 (2007) 753–766
JOURNAL OF SOUND AND VIBRATION
www.elsevier.com/locate/jsvi

A finite element based investigation on obtaining high material damping over a large frequency range in viscoelastic composites

Rabindra Kumar Patel, Bishakh Bhattacharya, Sumit Basu*

Department of Mechanical Engineering, Indian Institute of Technology Kanpur, Kanpur 208016 UP, India

Received 8 September 2006; received in revised form 31 January 2007; accepted 4 February 2007
Available online 30 March 2007

Abstract

Various vibration and noise suppression applications require a high loss factor ($\tan\delta$) over a wide frequency range. Homopolymers often do not meet this requirement. However, the damping properties of polymeric composites can be modulated to achieve this goal. In this paper, we devise a simple finite element based unit cell model to calculate the effective $\tan\delta$ of a composite as a function of frequency. Using this method, we show that if the relaxation times of the constituents are properly chosen, a flat $\tan\delta$ response over a wide frequency range can be obtained. Inclusions with multiple layers are seen to be particularly suitable towards this end.

1. Introduction

Vibration and noise suppression applications include building structures under seismic excitation or wind loads [1], and railways [2] where mechanical vibrations of a wide frequency range are generated. Vibration of structures for general kind of loads, occur from about 0.1 Hz to 10 kHz depending on the size of the structure [3]. Ideal damping applications should provide a high loss factor $\tan\delta$ (either material or structural) over the entire range.

To achieve effective damping over a wide frequency range, various methods are used. Active [4] and semi-active vibration control techniques [5] magnetic vibration dampers [6] and particle dampers [7] can achieve high damping over wide range of frequencies. However, active damping usually suffers from spillover/waterbed effects [8,9]. Magnetic and particle vibration dampers have larger weight penalty.

Passive damping using viscoelastic materials is simpler to implement and more cost-effective than semi-active and active techniques [10]. A US patent shows that a viscoelastic medium with fibres dispersed throughout eliminates the need for a constraining layer, thus reducing the size and weight of a damping treatment [11].

As is well known, homopolymers exhibit a high material damping response over a relatively narrow range of temperature and frequency. Methods used for achieving a wide $\tan\delta$ vs. frequency response include the use of copolymers, blending with other polymers [12], or inorganic materials [13]. A more recent development is the

*Corresponding author. Tel.: +91 512 2597506; fax: +91 512 2597408.
E-mail address: sbasu@iitk.ac.in (S. Basu).

0022-460X/$ - see front matter © 2007 Elsevier Ltd. All rights reserved.
doi:10.1016/j.jsv.2007.02.010

interpenetrating polymer network (IPN) which is a novel class of polymer alloys where two or more crosslinked polymers are held together by physical entanglements [14]. A particularly interesting member of this group of materials is the gradient IPN, where a broad $\tan\delta$ over a temperature range of 273–373 K has been reported [15]. It should be noted that a gradient polymer can be treated as a polymer composite with a large number of viscoelastic phases.

In order to estimate the effective $\tan\delta$ of a polymeric composite, homogenization techniques have been extensively used. Hashin [16] has given bounds for macroscopic moduli of two or multiphase elastic heterogeneous materials. Later he extended the analysis to predict the macroscopic behaviour of heterogeneous linear viscoelastic media [17]. Christensen [18] has also derived analytical expressions for upper and lower bounds of the effective complex shear modulus of a linear viscoelastic matrix containing spherical voids or perfectly rigid spherical inclusions. Better estimates of the macroscopic viscoelastic properties can be obtained by using the Mori-Tanaka model [19] or other mean-field homogenization schemes [20]. Unit cell techniques used within the framework of the finite element (FE) method [19,20] offers an alternate route towards determining the effective loss and storage moduli as well as $\tan\delta$ of viscoelastic composites. Microstructure design for optimal damping performance has been attempted by Yi et al. [21,22] using asymptotic homogenization techniques.

The first objective of this work is to develop a simple computational technique for determining effective $\tan\delta$ of a polymeric composite material (given its morphology) from unit cell analysis. Additionally, using the devised technique we show that by carefully selecting the viscoelastic properties of the constituents, the $\tan\delta$ vs. frequency response of the composite can be suitably modulated. This aids in realizing the aim of obtaining a high $\tan\delta$ value over a wide range of frequencies. To this end specially engineered inclusions which themselves contain a number of layers with varying damping properties are found to be especially suitable.

In this paper performance of the material has been judged only on the basis of its material loss factor. Maximizing the overall damping performance of a free or constrained layer damping system depends on the material damping response of the viscoelastic layer [23]. In fact, as shown by Kerwin and Ungar [23], multiple, continuous or segmented constrained or free viscoelastic layer damping is an effective way of designing damping treatments. In such treatments the system loss factor depends sensitively on the material loss factor. However, it should be borne in mind that several situations arise where the maximum loss factor is not the only design criterion of interest.

The present paper is organized in the following way. Sections 2.1 and 2.2 explains the computational procedure adopted for solving a viscoelastic initial-boundary value problem using FE techniques. In Section 2.3 we outline the simple procedure adopted for extracting $\tan\delta$ of the composite from a unit cell analysis. Salient results obtained using this technique on a simple morphology are presented in Sections 3.1 and 3.2.

2. Computational procedure

In this work an initial/boundary value problem (IVBP) has been solved, for evaluating the effective damping behaviour of viscoelastic heterogeneous materials. Variables of state which are used to assess the response of material are displacement $\mathbf{u}(\mathbf{x},t)$, the stress tensor $\boldsymbol{\sigma}(\mathbf{x},t)$ and strain tensor $\boldsymbol{\varepsilon}(\mathbf{x},t)$. In absence of body forces the governing equation which has to be solved is

$$\boldsymbol{\nabla}\cdot\boldsymbol{\sigma}=\mathbf{0}. \tag{1}$$

Assuming small strains the strain–displacement relations are:

$$\boldsymbol{\varepsilon}=\tfrac{1}{2}(\boldsymbol{\nabla}\cdot\mathbf{u}+\boldsymbol{\nabla}\cdot\mathbf{u}^{\mathrm{T}}) \tag{2}$$

and the constitutive equation for viscoelastic medium reads

$$\boldsymbol{\sigma}=\int_{t_0}^{t}\mathbf{C}(\mathbf{x},t-t')\frac{\partial\boldsymbol{\varepsilon}(\mathbf{x},t')}{\partial t'}\,\mathrm{d}t', \tag{3}$$

where $\mathbf{C}(\mathbf{x},t)$ is the viscoelastic constitutive tensor, t_0 initial time, t time of observation, and t' is the variable of integration.

Constraints imposed on the solution by boundary and initial conditions are:

$$\mathbf{u} = \mathbf{u}_0 \quad \text{on } \Gamma_u, \tag{4}$$

$$\mathbf{T} = \boldsymbol{\sigma}^{\mathrm{T}}\mathbf{n} = \mathbf{T}_0 \quad \text{on } \Gamma_t, \Gamma_u \cup \Gamma_t = 0, \tag{5}$$

where $\mathbf{T}_0$ is the applied traction on Γ_t. On the remaining part of the boundary (i.e. Γ_u) displacement $\mathbf{u}_0$ is specified, and $\mathbf{n}$ is unit normal to the boundary, as shown in Fig. 1.

For $t < t_0$,

$$\mathbf{u}(\mathbf{x}, t) = \mathbf{0} \quad \text{and} \quad \boldsymbol{\sigma}(\mathbf{x}, t) = \mathbf{0}. \tag{6}$$

2.1. Incremental form of the constitutive equation

In order to avoid solving a set of Volterra integrals for the FE solution, numerical incrementalization of the constitutive equation developed by Zocher et al. [24] has been used in this formulation. Use of this numerically approximated constitutive equation leads to a simple set of algebraic equations. Steps involved in deriving the incremental constitutive equation are outlined here for the sake of completeness.

The time line is subdivided into discrete intervals such that $t_{n+1} = t_n + \Delta t$. At the nth and $(n+1)$th time steps the constitutive relations are given by

$$\boldsymbol{\sigma}(\mathbf{x}, t_n) = \int_0^{t_n} \mathbf{C}(\mathbf{x}, t_n - t') \frac{\partial \boldsymbol{\varepsilon}(\mathbf{x}, t')}{\partial t'} \, \mathrm{d}t' \tag{7}$$

and

$$\boldsymbol{\sigma}(\mathbf{x}, t_{n+1}) = \int_0^{t_{n+1}} \mathbf{C}(\mathbf{x}, t_{n+1} - t') \frac{\partial \boldsymbol{\varepsilon}(\mathbf{x}, t')}{\partial t'} \, \mathrm{d}t', \tag{8}$$

respectively.

Eq. (8) can also be written as

$$\boldsymbol{\sigma}(\mathbf{x}, t_{n+1}) = \int_0^{t_n} \mathbf{C}(\mathbf{x}, t_{n+1} - t') \frac{\partial \boldsymbol{\varepsilon}(\mathbf{x}, t')}{\partial t'} \mathrm{d}t' + \int_{t_n}^{t_{n+1}} \mathbf{C}(\mathbf{x}, t_{n+1} - t') \frac{\partial \boldsymbol{\varepsilon}(\mathbf{x}, t')}{\partial t'} \mathrm{d}t'. \tag{9}$$

Here, we define $\Delta\boldsymbol{\sigma}$ as

$$\Delta\boldsymbol{\sigma} = \boldsymbol{\sigma}(\mathbf{x}, t_{n+1}) - \boldsymbol{\sigma}(\mathbf{x}, t_n), \tag{10}$$

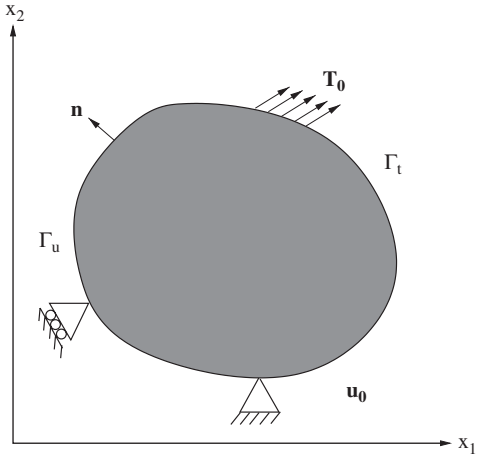

Fig. 1. Two-dimensional problem domain.

and $\Delta\mathbf{C}$ as

$$\Delta\mathbf{C} = \mathbf{C}(\mathbf{x}, t_{n+1} - t') - \mathbf{C}(\mathbf{x}, t_n - t'). \tag{11}$$

In the above $\mathbf{C}$ is fitted with Wiechert model in the form

$$\mathbf{C}(\mathbf{x}, t - t') = \mathbf{C}_\infty + \sum_{r=1}^{N} \mathbf{C}_r \exp(-(t - t')/\rho_r), \tag{12}$$

where the quantity N in represents number of spring–dashpot combinations in the model. Substituting Eqs. (7) and (9) in Eq. (10), $\Delta\boldsymbol{\sigma}$ can be expressed as

$$\Delta\boldsymbol{\sigma} = \int_0^{t_n} (\mathbf{C}(\mathbf{x}, t_{n+1} - t') - \mathbf{C}(\mathbf{x}, t_n - t')) \frac{\partial\boldsymbol{\varepsilon}(\mathbf{x}, t')}{\partial t'} \mathrm{d}t' + \int_{t_n}^{t_{n+1}} \mathbf{C}(\mathbf{x}, t_{n+1} - t') \frac{\partial\boldsymbol{\varepsilon}(\mathbf{x}, t')}{\partial t'} \mathrm{d}t'. \tag{13}$$

Therefore,

$$\Delta\boldsymbol{\sigma} = \int_{t_n}^{t_{n+1}} \mathbf{C}(\mathbf{x}, t_{n+1} - t') \frac{\partial\boldsymbol{\varepsilon}(\mathbf{x}, t')}{\partial t'} \, \mathrm{d}t' + \Delta\boldsymbol{\sigma}^{\mathrm{R}} \tag{14}$$

where

$$\Delta\boldsymbol{\sigma}^{\mathrm{R}} = \int_0^{t_n} \Delta\mathbf{C} \frac{\partial\boldsymbol{\varepsilon}(\mathbf{x}, t')}{\partial t'} \, \mathrm{d}t'. \tag{15}$$

For the plane strain case, in which we are particularly interested,

$$\mathbf{C}_\infty = \frac{E_\infty}{(1+v)(1-2v)} \begin{pmatrix} (1-v) & v & 0 \\ v & (1-v) & 0 \\ 0 & 0 & (1-2v) \end{pmatrix}, \tag{16}$$

and

$$\mathbf{C}_r = \frac{E_r}{(1+v)(1-2v)} \begin{pmatrix} (1-v) & v & 0 \\ v & (1-v) & 0 \\ 0 & 0 & (1-2v) \end{pmatrix}, \tag{17}$$

where E_∞ is the long-term relaxation modulus, and v, the Poisson's ratio is assumed to be time independent. In addition, $\rho_r = \eta_r/E_r$, where η_r are dashpot coefficients and E_r are spring stiffnesses of the rth spring–dashpot combination in the Wiechert model. The ρ_r are referred to as relaxation times.

Eq. (14) can be further integrated in closed form to produce:

$$\Delta\boldsymbol{\sigma} = \mathbf{C}'\Delta\boldsymbol{\varepsilon} + \Delta\boldsymbol{\sigma}^{\mathrm{R}}, \tag{18}$$

where

$$\mathbf{C}' = \mathbf{C}_\infty + \frac{1}{\Delta t} \sum_{r=1}^{N} \rho_r \mathbf{C}_r (1 - \exp(-\Delta t/\rho_r)) \tag{19}$$

and

$$\Delta\boldsymbol{\sigma}^{\mathrm{R}} = -\sum_{r=1}^{N} (1 - \exp(-\Delta t/\rho_r)) \int_0^{t_n} \exp(-(t_{n+1} - t')/\rho_r) \mathbf{C}_r \frac{\partial\boldsymbol{\varepsilon}(\mathbf{x}, t')}{\partial t'} \, \mathrm{d}t'. \tag{20}$$

Eqs. (18)–(20) form the corner stone of the incremental FE formulation. Note that $\mathbf{C}'$ a constant (as in a linear elastic analysis) if the time step Δt is fixed.

For the time interval $(t_n - \Delta t \leqslant t' \leqslant t_n)$ the strain rate $\mathbf{R}$ is approximated as

$$\frac{\partial\boldsymbol{\varepsilon}(\mathbf{x}, t')}{\partial t'} \simeq \frac{\Delta\boldsymbol{\varepsilon}}{\Delta t} \simeq \mathbf{R}.$$

Now Eq. (20) can be simplified to

$$\Delta\boldsymbol{\sigma}^{\mathrm{R}} = -\sum_{r=1}^{N}(1-\exp(-\Delta t/\rho_r))\mathbf{S}_r(\mathbf{x},t_n), \tag{21}$$

where again for plane strain conditions,

$$\mathbf{S}_r(\mathbf{x},t_n) = \int_0^{t_n} \exp(-(t_{n+1}-t')/\rho_r) \tag{22}$$

$$\times\frac{E_r}{(1+v)(1-2v)}\begin{pmatrix}(1-v) & v & 0\\ v & (1-v) & 0\\ 0 & 0 & (1-2v)\end{pmatrix}\mathbf{R}\,\mathrm{d}t'. \tag{23}$$

In addition, the $\mathbf{S}_r(\mathbf{x},t_n)$ satisfies the recursive relation,

$$\mathbf{S}_r(\mathbf{x},t_n) = \exp(-\Delta t/\rho_r)\mathbf{S}_r(\mathbf{x},t_{n-1}) + (1-\exp(-\Delta t/\rho_r))\frac{E_r\rho_r}{(1+v)(1-2v)}\begin{pmatrix}(1-v) & v & 0\\ v & (1-v) & 0\\ 0 & 0 & (1-2v)\end{pmatrix}\mathbf{R}. \tag{24}$$

2.2. Finite element formulation

In absence of body forces, virtual work rate equation for small deformation can be written as

$$\int_V \delta\dot{\boldsymbol{\varepsilon}}^{\mathrm{T}}\boldsymbol{\sigma}\,\mathrm{d}V = \int_S \delta\mathbf{v}^{\mathrm{T}}\mathbf{T}\,\mathrm{d}S. \tag{25}$$

Usual FE assumptions are made as

$$\mathbf{v}(\mathbf{x},t) = \mathbf{N}\dot{\mathbf{U}} \tag{26}$$

and

$$\dot{\boldsymbol{\varepsilon}}(\mathbf{x},t) = \mathbf{B}\dot{\mathbf{U}}, \tag{27}$$

within each element, where $\mathbf{U}$ is the vector of nodal displacements, $\mathbf{N}$ is the shape function matrix and $\mathbf{B}$ is the strain–displacement matrix.

Standard FE procedures for small strain leads to the incremental equation,

$$\int_V \mathbf{B}^{\mathrm{T}}\Delta\boldsymbol{\sigma}\,\mathrm{d}V = \int_S \mathbf{N}^{\mathrm{T}}\Delta\mathbf{T}\,\mathrm{d}S. \tag{28}$$

With the use of Eq. (18), Eq. (28) becomes,

$$\int_V \mathbf{B}^{\mathrm{T}}(\mathbf{C}'\Delta\boldsymbol{\varepsilon}+\Delta\boldsymbol{\sigma}^{\mathrm{R}})\,\mathrm{d}V = \int_S \mathbf{N}^{\mathrm{T}}\Delta\mathbf{T}\,\mathrm{d}S, \tag{29}$$

which, in turn, can be written as

$$\int_V \mathbf{B}^{\mathrm{T}}\mathbf{C}'\mathbf{B}\Delta\mathbf{U}\,\mathrm{d}V + \int_V \mathbf{B}^{\mathrm{T}}\Delta\boldsymbol{\sigma}^{\mathrm{R}}\mathrm{d}V = \int_S \mathbf{N}^{\mathrm{T}}\Delta\mathbf{T}\,\mathrm{d}S, \tag{30}$$

or

$$\mathbf{K}\Delta\mathbf{U} = \Delta\mathbf{F} - \Delta\boldsymbol{\chi}, \tag{31}$$

where $\mathbf{K} = \int_V \mathbf{B}^{\mathrm{T}}\mathbf{C}'\mathbf{B}\,\mathrm{d}V$, is the global stiffness matrix. The first term on the right-hand side of Eq. (31) is the vector containing the external load increments, and $\Delta\boldsymbol{\chi}$ is the time-dependent contribution due to viscoelasticity.

2.3. Unit cell technique

One of the objectives of this work is to determine the effective damping factor $\tan\delta^c$ of a microstructured material. To this end a unit cell technique is employed. The unit cell, which in principle may represent any microstructure, is subjected to special boundary conditions that ensure that "straight edges remain straight". The Rayleigh–Ritz technique used to implement these boundary conditions are as outlined in Ref. [25], while more general periodic boundary conditions have been given in Refs. [26,27]. Though the above formulation does not restrict the morphology of the composite, in this preliminary analysis we adopt a square arrangement of cylindrical inclusions with cross-section as shown in Fig. 2(a). In view of the reflective and translational symmetries, the shaded unit cell can be simplified to the one shown in Fig. 2(b). Note that symmetry boundary conditions are imposed on the edges $x_1 = 0$ and $x_2 = 0$. Results presented in the next section all pertain to this particular morphology. The unit cell is subjected to (see Fig. 2(b)) uniform normal macrostresses,

$$\Sigma_1(t) = \frac{1}{H}\int_0^H \sigma_{11}(t)\,\mathrm{d}x_2 \quad \text{and} \quad \Sigma_2(t) = \frac{1}{B}\int_0^B \sigma_{22}(t)\,\mathrm{d}x_1, \tag{32}$$

where $\sigma_{ij}(t)$ are microstresses. The $\tan\delta^c$ can be obtained in the following way. Consider a macrostress state $\Sigma_2(t) = 0$ and $\Sigma_1(t) = \Sigma_0 \sin\omega t$. Then for a viscoelastic material, the macrostrain response $\bar{\varepsilon}_1$ is given by

$$\bar{\varepsilon}_1 = \frac{1}{BH}\int_V \varepsilon_{11}(t)\,\mathrm{d}V, \tag{33}$$

lags the macrostress by a time $\Delta\tau$ as shown in Fig. 2(c). When $t \gg$ the largest relaxation time the effective damping factor becomes,

$$\tan\delta^c = \tan(\omega\Delta\tau). \tag{34}$$

Four noded quadrilateral elements are used to model the unit cells in all cases reported. Further details of the Rayleigh–Ritz technique adopted are given in Appendix A.

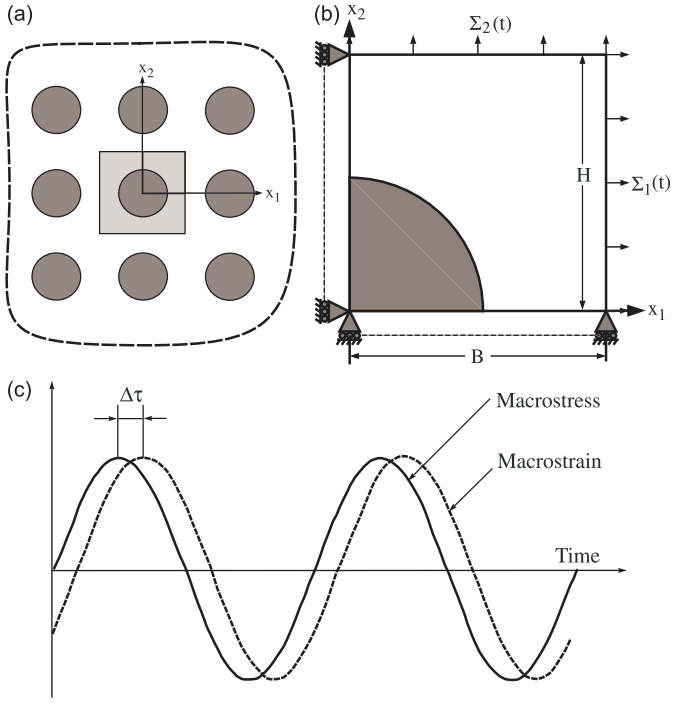

Fig. 2. Schematic diagrams showing (a) the square arrangement of cylindrical inclusions and the unit cell. The domain analysed by FEM is shown in (b). The effective $\tan\delta^c$ is calculated from the phase difference between the macrostress and macrostrain responses as shown in (c).

3. Results and discussion

In this section, we analyse composites with viscoelastic matrices and elastic or viscoelastic inclusions using the FE technique outlined above. The objective of the results presented hereafter is to provide a 'proof of concept' of the fact that the damping response of a composite can be 'designed' appropriately by a suitable choice of viscoelastic material properties of the constituents.

In particular, we demonstrate that, by adding suitable inclusions in a matrix, it is possible in principle to modify its damping response to be high over a wide frequency range. To this end, the simple microstructure described in Section 2.3 will be used.

Since our purpose is to provide a 'proof of concept', we use the standard linear solid (SLS) with a one term Prony series representation, $E(t) = E_\infty + E_1 e^{-t/\rho_1}$ (see Eq. (12)).

In this work, the superscript 'm' is used to denote matrix quantities and 'c' for effective quantities pertaining to the composite. Superscript 'p_1', 'p_2', etc. are used for the reinforcing phases. Thus, Prony series representations of the moduli of the matrix, first phase and second phase of the composite are $E^m(t) = E^m_\infty + E^m_1 e^{-t/\rho^m_1}$, $E^{p_1}(t) = E^{p_1}_\infty + E^{p_1}_1 e^{-t/\rho^{p_1}_1}$, and $E^{p_2}(t) = E^{p_2}_\infty + E^{p_2}_1 e^{-t/\rho^{p_2}_1}$ whereas that for $\tan\delta$ are $\tan\delta^m$, $\tan\delta^{p_1}$ and $\tan\delta^{p_2}$, respectively. For the composite, the effective $\tan\delta$ is denoted by $\tan\delta^c$.

3.1. Effective damping response of composites

For a SLS having modulus of the form $E(t) = E_\infty + E_1 e^{-t/\rho_1}$, a simple calculation shows that the maximum attainable $\tan\delta$ is $0.5(R^2 + R)^{-1/2}$, which is achieved at a frequency of $\sqrt{(R)}/(2\pi\rho_1\sqrt{(1+R)})$ Hz, where $R = E_\infty/E_1$.

The approximate response of this SLS, when reinforced with inclusions can be obtained by applying the correspondence principle to the Voigt or Reuss estimates for the effective moduli. More sophisticated homogenization schemes are also available [19,20]. Thus, applying the correspondence principle to the Voigt estimate, for a two-phase composite, the $\tan\delta^c$ is given by

$$\tan\delta^c = \left(v^{p_1}\tan\delta^{p_1} + v^m\frac{E'^m}{E'^{p_1}}\tan\delta^m\right)\Big/\left(v^{p_1} + \frac{E'^m}{E'^{p_1}}v^m\right), \tag{35}$$

where v^{p_1}, v^m and E'^{p_1}, E'^m volume fractions and storage moduli of inclusion and matrix, respectively. For SLS, E'^{p_1} and E'^m can be expressed as

$$E'^{p_1} = E^{p_1}_\infty + E^{p_1}_1\frac{\omega^2(\rho^{p_1}_1)^2}{1+\omega^2(\rho^{p_1}_1)^2}$$

and

$$E'^m = E^m_\infty + E^m_1\frac{\omega^2(\rho^m_1)^2}{1+\omega^2(\rho^m_1)^2},$$

respectively. Using the above estimate, the $\tan\delta^c$ response is plotted for a particular pair of viscoelastic materials in Fig. 3, where it is clear that the peaks of the $\tan\delta^c$ vs. ω response now occurs at two values of ω instead of one. For comparison, the estimate of $\tan\delta^c$ based on a closer estimate for the moduli of a composite with unidirectional fibres running in the out-of-plane direction (as shown in Table 8.1 of Ref. [29]) is also shown with dashed lines. Even from this more exact estimate, two peaks do appear in the $\tan\delta^c$ response though the height of the peaks are different from the Voigt estimate. The location of the peaks in frequency is same in the two estimates.

However, if the added inclusions are elastic (i.e. $E^{p_1}_1 = 0$), always $\tan\delta^c \leqslant \tan\delta^m$. This is demonstrated in Fig. 4 on the basis of the Voigt estimate. We now define a quantity α as

$$\alpha = \frac{\max(\tan\delta^c)}{\max(\tan\delta^m)}. \tag{36}$$

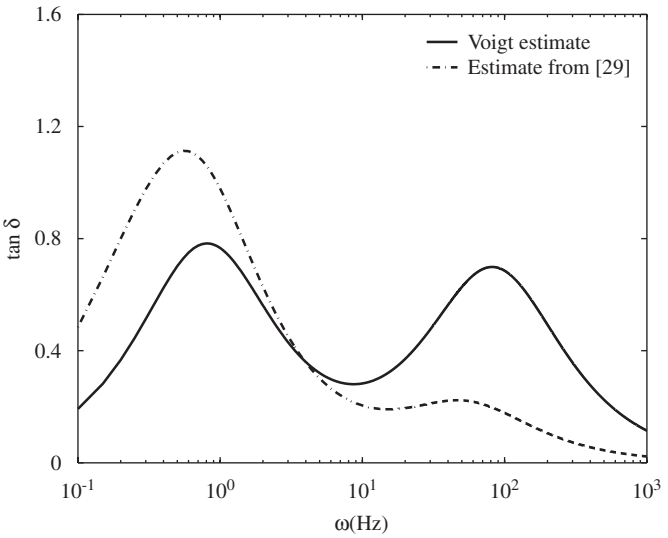

Fig. 3. Voigt estimate for two phase viscoelastic composite, with $E^m(t) = 1 + 15e^{-t/0.001}$ Mpa and $E^{p_1}(t) = 1 + 10e^{-t/0.1}$ Mpa, $v^{p_1} = 0.3$ (solid curve) and a more exact estimate (dashed curve) based on application of correspondence principle to the effective moduli given in Table 8.1 of Ref. [29]. Peaks occur almost at same frequencies in both cases.

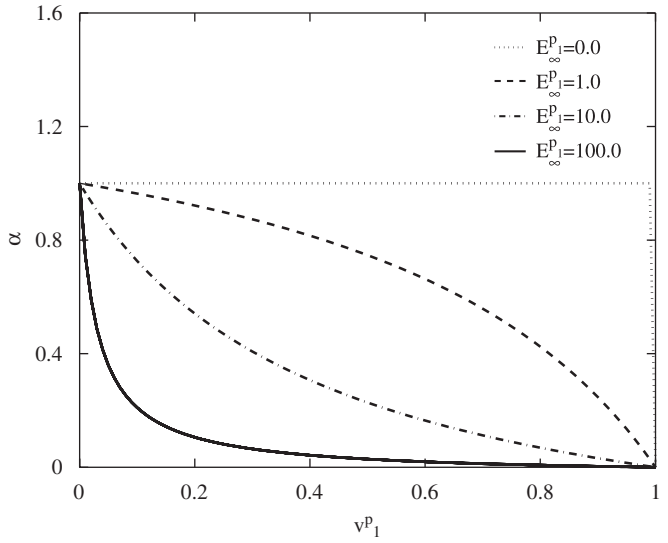

Fig. 4. Variation of $\alpha = \max(\tan\delta^c)/\max(\tan\delta^m)$ with volume fraction v^{p_1} of two phase viscoelastic–elastic composites as obtained from simple Voigt estimate.

In Fig. 4, the variation of α has been plotted against v^{p_1}. The maximum damping achievable in the composite for $E^{p_1}_\infty \neq 0$ is always lower than that of the matrix. In fact, with increase in v^{p_1} and $E^{p_1}_\infty$, α drops significantly below unity. Also when $E^{p_1}_1 = 0$, Eq. (35) shows only one peak instead of two.

To achieve $\alpha > 1$ we need to use viscoelastic inclusions, i.e. $E^{p_1}_1 \neq 0$. This is demonstrated in Fig. 5 where again α has been plotted against $E^m_1/E^{p_1}_1$ for a viscoelastic–viscoelastic composite. Clearly, according to the Voigt estimate, for $E^m_1/E^{p_1}_1 \lesssim 1.5$, $\alpha > 1$ is achievable. Thus Figs. 4 and 5 demonstrate that achieving high damping capacity and stiffness are somewhat contradictory objectives. While elastic inclusions help us to achieve the latter, they are rather ineffective as damping enhancers [28].

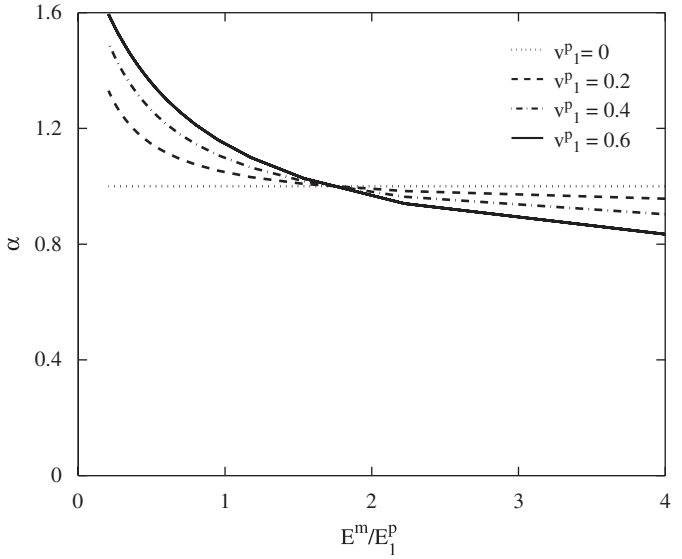

Fig. 5. Variation of $\alpha = \max(\tan\delta^c)/\max(\tan\delta^m)$ with $E_1^m/E_1^{p_1}$ for two phase viscoelastic–viscoelastic composites as obtained from simple Voigt estimate.

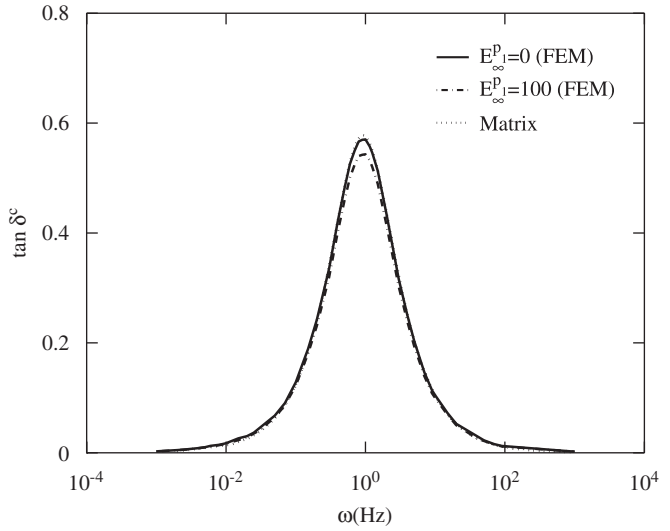

Fig. 6. Variation of effective $\tan\delta^c$ with ω for composites with 30% volume fraction of elastic inclusions ($E_\infty^{p_1} = 100\,\text{MPa}$) and 30% of void ($E_\infty^{p_1} = 0\,\text{MPa}$).

3.2. Modulation of the $\tan\delta$ vs. ω response of composites

We now turn to the results of actual FEM unit cell calculations where a square arrangement of cylindrical inclusions has been used. Fig. 6 shows the $\tan\delta - \omega$ response of the matrix with $E^m(t) = 1 + 2e^{-t/0.1}$ MPa and Poisson's ratio $v^m = 0.33$. Expectedly, $\tan\delta^m$ peaks at a frequency of $\omega = 0.9$ Hz and $\max(\tan\delta^m) = 0.5773$. It should be noted that the Poisson's ratio chosen represents a glassy polymer and a polymer in the rubbery regime has Poisson's ratio of 0.5.

Addition of elastic inclusions with $E_\infty^{p_1} = 100\,\text{MPa}$ and $v^{p_1} = 0.33$, again expectedly causes $\max(\tan\delta^c)$ to drop. On the other hand if 30% of the composite is voided (continuous curve in Fig. 6), there is almost no

modification of the max($\tan\delta^c$) value over max($\tan\delta^m$). These results are in keeping with the predictions presented on the basis of the simple Voigt estimates.

The product of the stiffness $|E^c| = |E'^c + iE''^c|$ (E'^c and E''^c are the storage and loss moduli of the composite) and $\tan\delta^c$ has been plotted in Fig. 7. Lakes [28] considers this quantity to be a proper figure of merit for damping materials. Fig. 7 shows that $|E^c|\tan\delta^c$ is much higher for the composite with elastic inclusions, compared to the matrix. This figure underlines the beneficial effect of using elastic inclusions as a means of achieving a judicious compromise between stiffness and damping properties. However, elastic inclusions are not considered further in this paper as they are ineffective in flattening the $\tan\delta^c$ response.

Shape of the inclusions however, has a significant effect on $\tan\delta^c$. The effect of variation in $\tan\delta^c$ with shape is obviously not captured by the simple Voigt model (see Figs. 3–5). A somewhat better idea about the effect of shape is afforded by Fig. 8, where $\tan\delta^c$ is presented as a function of v^{p_1} for different shapes of inclusions. The results are obtained from unit cell simulations using the four morphologies shown in the inset. Cross-sections of inclusions which are more elongated along the direction of loading (i.e. x_1) give the highest $\tan\delta^c$. On the other hand, cross-sections of the inclusions that are elongated in a direction perpendicular to the load yield the least $\tan\delta^c$ values. Thus for elliptical inclusions (d) shows a much lower $\tan\delta^c$ than (c).

From the discussion above, it is clear that elastic inclusions (or voids) are not very beneficial in modifying the damping of the composite. Shape and morphology control, (to an extent more sophisticated than what is attempted here) may lead to somewhat improved $\tan\delta^c$. However, widening of the $\tan\delta^c - \omega$ response is not possible by controlling only the shape or the elastic properties of the inclusions. This view is supported both by detailed FEM calculations as well as by simple Voigt estimates of $\tan\delta^c$.

The principle of flattening the $\tan\delta^c - \omega$ response is simple and is demonstrated here. Fig. 9 shows the responses of the matrix and composites. The matrix properties are $E^m(t) = 1 + 2e^{-t/0.1}$ Mpa (same as in Fig. 6) while the inclusions have $E^{p_1}(t) = 1 + 30e^{-t/0.0005}$ MPa. Note that in the example chosen, $\rho_1^m/\rho_1^{p_1} = 200$. Simple calculation shows that the frequency corresponding to the $\tan\delta$ peak for the matrix occurs at $\omega^m = 0.9$ Hz and for inclusion at $\omega^{p_1} = 57$ Hz. The $\tan\delta^c - \omega$ response of the composite with $v^{p_1} = 0.3$ exhibits two distinct peaks at $\omega_1^c = 1$ Hz and $\omega_2^c = 40$ Hz. This is due to the fact that ρ^m and ρ^{p_1} are spaced such that $|1/\rho^m - 1/\rho^{p_1}| \gg$ bandwidth of either the matrix or the inclusion. If this condition is not satisfied, two distinct peaks do not result.

The flattening of the response in Fig. 9 can be achieved by adding sufficient volume fraction of a third phase with a relaxation time ρ^{p_2} such that,

$$\rho^{p_1} \leqslant \rho^{p_2} \leqslant \rho^m. \tag{37}$$

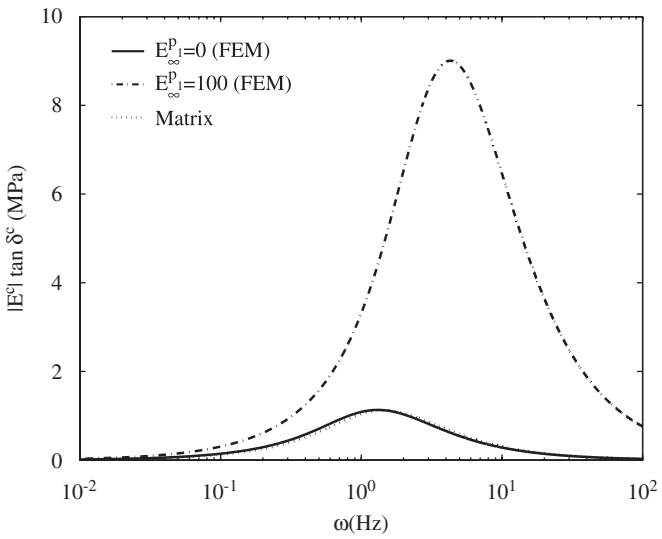

Fig. 7. Variation of $|E^c|\tan\delta^c$ with ω of composites with 30% volume fraction of elastic inclusions ($E_\infty^{p_1} = 100$ MPa) and 30% of voids ($E_\infty^{p_1} = 0$ MPa).

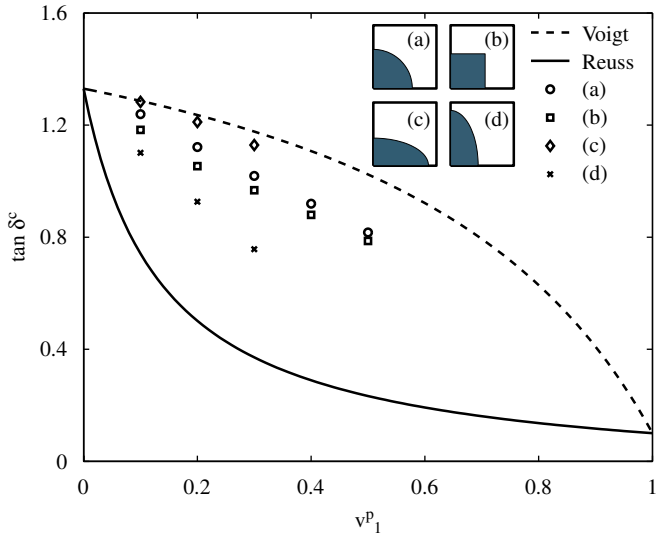

Fig. 8. Variation of $\tan\delta^c$ with volume fraction v^{p_1} of inclusions with various cross-sectional shapes. The Voigt and Reuss bounds are also shown.

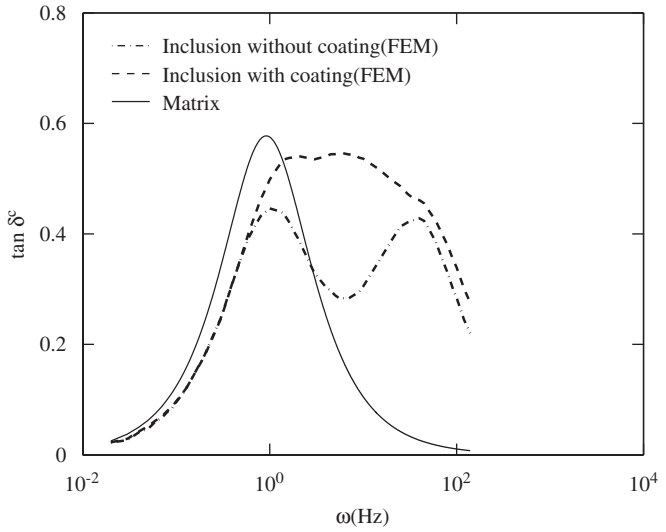

Fig. 9. Variation of $\tan\delta^c$ with ω of viscoelastic inclusion with and without viscoelastic coatings. The $\tan\delta^m$ vs. ω response of the matrix is also shown.

To demonstrate this, we have used a coating of a third material on the inclusion. The coating has properties $E^{p_2}(t) = 1 + 20e^{-t/0.005}$ Mpa and $v^{p_2} = 0.25$ where ρ^{p_2} is in accordance with Eq. (37). The coating may represent the interphase region that exists between inclusion and matrix in polymeric composites [19]. Addition of the coating leads to a flatter response of $\tan\delta^c$ shown in Fig. 9. Thus, by using a 3-phase viscoelastic composite, a reasonably flat $\tan\delta^c$ response is obtained over the 1–100 Hz frequency range with a sacrifice in peak value in the range of 5%. The flatness is achieved primarily by spacing the relaxation times of the constituents appropriately. Further the volume fractions and thus morphology also need to be adjusted.

In principle, flatness of $\tan\delta^c$ over a larger frequency range can also be achieved by this technique. This can be done by simply using multiphase materials (e.g. a graded IPN) with a wide range of relaxation times.

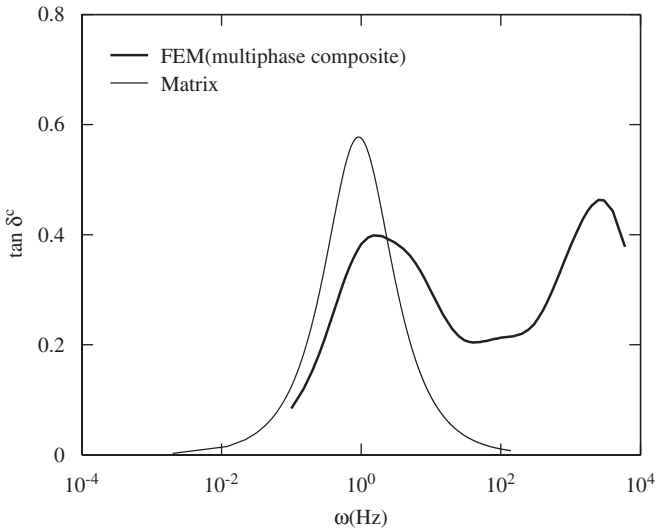

Fig. 10. Variation of $\tan\delta^c$ with ω for a viscoelastic composite with layered inclusions. The $\tan\delta^m$ vs. ω response of the matrix is also shown.

In Fig. 10 we show the results obtained for a fictitious composite material that has inclusions with graded relaxation times. Here we demonstrate the first attempts at morphology control to achieve a flat $\tan\delta^c$ response over a large frequency range. In this figure three additional phases have been used. These phases are arranged in concentric circles around phase p_1. All these four phases have almost similar moduli but their relaxation times range from 10^{-5} to 10^{-2} s. The matrix properties remain the same as in Figs. 6 and 9. The response obtained for this multiphase composite is reasonably high over the range 1–10^4 Hz. The flatness of the curve over this entire range however cannot be ensured without optimizing the volume fractions v^{p_n} and moduli $E_1^{p_n}$ of the phases. We are currently working on a systematic procedure for performing this optimization.

4. Conclusion

In this work a unit cell based FE procedure for determining the effective $\tan\delta^c$ response of multiphase composite materials is proposed.

The procedure is applied to the determination of $\tan\delta^c$ for simple morphologies of polymeric composites with SLS constituents. In the process it is demonstrated that by judiciously choosing the viscoelastic constituents and their morphology, a flat $\tan\delta^c$ vs. ω response can be obtained over a wide frequency range. In particular, inclusions with multiple layers having different relaxation times are seen to be especially suitable for modulating the $\tan\delta^c$ response.

Appendix A

In this appendix the Rayleigh–Ritz procedure for the application of periodic boundary conditions on the unit cell shown in Fig. 2(b) have been described. The procedure adopted in this work is basically similar to that described in Ref. [25] and is included here for completeness.

The macrostress state $\mathbf{\Sigma}$ applied on the unit cell is assumed to be a principal stress state and hence the edges of the unit cell remain straight during deformation. Using reflection symmetry on the square lattice, only quarter of the unit cell needs to be analysed subject to the condition that

$$\Sigma_1(t) = \frac{1}{V}\int_V \sigma_{11}\,\mathrm{d}V = \frac{1}{H}\int_0^H \sigma_{11}\,\mathrm{d}x_2$$

and

$$\Sigma_2(t) = \frac{1}{V}\int_V \sigma_{22}\,\mathrm{d}V = \frac{1}{B}\int_0^B s\sigma_{22}\,\mathrm{d}x_1, \tag{38}$$

where $\boldsymbol{\sigma}$ is the microstress inside the unit cell domain.

The boundaries of the unit cell are maintained straight subject to satisfaction of Eq. (38) by the following technique.

The total vector $\Delta\mathbf{U}$ of nodal displacement in Eq. (31) can be partitioned as

$$\Delta\mathbf{U} = [\Delta\mathbf{u}_I; \Delta\mathbf{u}_{II}; \Delta\mathbf{w}]^{\mathrm{T}}, \tag{39}$$

where $\Delta\mathbf{u}_I$ contains the horizontal nodal displacement increments along $x_1 = H$ (all such displacements increments have magnitude ΔU_I), while the vector $\Delta\mathbf{u}_{II}$ contains the vertical nodal displacement increments along $x_2 = B$ (all having magnitude ΔU_{II}) as shown in Fig. 2(b). The vector $\Delta\mathbf{w}$ contains all remaining nodal displacement increments. The Rayleigh–Ritz procedure basically determines the magnitudes ΔU_I and ΔU_{II} from the conditions that the corresponding average macrostresses in x_1 and x_2 directions retain specified values $\Sigma_1(t)$ and $\Sigma_2(t)$, which are in our case sinusoidally varying with time and zero respectively.

To this end, three trial solutions are performed at each time step of the solution procedure, i.e. solution to Eq. (31) is obtained by the following procedure:

1. A unit incremental displacement is given along $x_1 = H$, with $\Delta\mathbf{F} = \Delta\boldsymbol{\chi} = 0$. The result of this exercise is a displacement vector $\Delta\mathbf{U}_1$.
2. A unit incremental displacement is given along $x_2 = B$, with $\Delta\mathbf{F} = \Delta\boldsymbol{\chi} = 0$. The result of this exercise is a displacement vector $\Delta\mathbf{U}_2$.
3. The vertical displacement along $x_1 = H$ and the horizontal displacement along $x_2 = B$ are held at zero while Eq. (31) are solved with $\Delta\boldsymbol{\chi}$. The result of this exercise is a third displacement vector $\Delta\mathbf{U}_3$.

The final solution can then be written as

$$\Delta\mathbf{U} = \sum_{i=1}^{3} \alpha_i \Delta\mathbf{U}_i, \tag{40}$$

where $\alpha_1 \equiv \Delta U_I$, $\alpha_2 \equiv \Delta U_{II}$, and $\alpha_3 \equiv 1$. Substituting $\Delta\mathbf{U}$ in Eq. (31),

$$\sum_{j=1}^{3} \alpha_j \mathbf{K}\Delta\mathbf{U}_j = \Delta\mathbf{F} - \Delta\boldsymbol{\chi} \tag{41}$$

and premultiplying the above equation by $\Delta\mathbf{U}_i$ gives a system of linear equations in α_i,

$$\sum_{j=1}^{3} r_{ij}\alpha_j = \Delta f_i - b_i, \tag{42}$$

where $r_{ij} = \Delta\mathbf{U}_i^{\mathrm{T}}\mathbf{K}\Delta\mathbf{U}_j$, $\Delta f_i = \Delta\mathbf{U}_i^{\mathrm{T}}\Delta\mathbf{F}$ and $b_i = \Delta\mathbf{U}_i^{\mathrm{T}}\Delta\boldsymbol{\chi}$. Rewriting above equation in matrix form

$$\begin{bmatrix} r_{11} & r_{12} & r_{13} \\ r_{21} & r_{22} & r_{23} \\ r_{31} & r_{32} & r_{33} \end{bmatrix} \begin{bmatrix} \Delta U_I \\ \Delta U_{II} \\ 1 \end{bmatrix} = \begin{bmatrix} \Delta f_1 \\ \Delta f_2 \\ \Delta f_3 \end{bmatrix} - \begin{bmatrix} b_1 \\ b_2 \\ b_3 \end{bmatrix}, \tag{43}$$

where $\Delta f_1 = \Delta\Sigma_1 A$, $\Delta f_2 = \Delta\Sigma_2 B$, and $\Delta f_3 = 0$. Now above equation can be solved for ΔU_I and ΔU_{II}, and final displacement increment can be obtained from Eq. (40).

References

[1] K. Ye, L. Li, J. Tang, Stochastic seismic response of structures with added viscoelastic dampers modeled by fractional derivative, *Earthquake Engineering and Engineering Vibration* 2 (2003) 133–139.

[2] A. Castellani, Vibrations generated by rail vehicles: a mathematical model in the frequency domain, *Vehicle System Dynamics* 34 (2000) 153–173.
[3] R.S. Lakes, *Viscoelastic Solids*, CRC Press, Boca Raton, FL, 1998.
[4] J.L. Jang, Y.S. Tarng, A study of the active vibration control of a cutting tool, *Journal of Materials Processing Technology* 95 (1999) 78–82.
[5] W. Taniwangsa, J.M. Kelly, Experimental testing of a semi-active control scheme for vibration suppression, *Proceedings of the SPIE—The International Society for Optical Engineering* 3045 (1997) 130–139.
[6] M. Hansaka, N. Mifune, Development of a new type high grade damper: magnetic-vibration-damper, *Quarterly Report of Railway Technical Research Institute (Japan)* 35 (1994) 199–201.
[7] W. Liu, G. Tomlinson, K. Worden, Nonlinearity study of particle dampers, *Proceedings of the 2002 International Conference on Noise and Vibration Engineering ISMA*, Leuven Belgium, September 2002, pp. 495–499.
[8] H. Sano, T. Inoue, A. Takahashi, K. Terai, Y. Nakamura, Active control system for low-frequency road noise combined with an audio system, *IEEE Transactions on Speech and Audio Processing* 9 (2001) 755–763.
[9] S. Raja, K. Rohwer, M. Rose, Modeling and active vibration control of laminated composite beams, *Journal of Intelligent Material Systems and Structures* 10 (1999) 890–899.
[10] M.D. Rao, Recent applications of viscoelastic damping for noise control in automobiles and commercial airplanes, *Journal of Sound and Vibration* 262 (2003) 457–474.
[11] E.A. Thomas, C. Yung, Fiber enhancement of viscoelastic damping polymers, U.S. Patent No. 5,256,223, 1993.
[12] G.S. Huang, L.X. Jiang, L. Qiang, Molecular design of damping rubber based on polyacrylate-containing silicone, *Journal of Applied Polymer Science* 85 (2002) 746–751.
[13] E. Vassileva, K. Friedrich, Epoxy/alumina nanoparticle composites: dynamic mechanical behaviour, *Journal of Applied Polymer Science* 89 (2003) 3774–3785.
[14] C.L. Qin, W.M. Cai, J. Cai, D.Y. Tang, J.S. Zhang, M. Qin, Damping properties and morphology of polyurethane/vinyl ester resin interpenetrating polymer network, *Materials Chemistry and Physics* 85 (2004) 402–409.
[15] Y. S Lipatov, L.V. Karabanova, Gradient interpenetrating polymer networks, *Journal of Materials Science* 30 (1995) 2475–2484.
[16] Z. Hashin, The elastic moduli of heterogeneous materials, *Journal of Applied Mechanics* 29 (1962) 143–150.
[17] Z. Hashin, Viscoelastic behaviour of heterogeneous media, *Journal of Applied Mechanics—Transactions of the ASME* 32E (1965) 630–663.
[18] R.M. Christensen, Viscoelastic properties of heterogeneous media, *Journal of the Mechanics and Physics of Solids* 17 (1969) 17–41.
[19] F.T. Fisher, L.C. Brinson, Viscoelastic interphases in polymer-matrix composites: theoretical models and finite-element analysis, *Composites Science and Technology* 61 (2001) 731–748.
[20] C. Friebel, I. Doghri, V. Legat, General mean-field homogenization schemes for viscoelastic composites containing multiple phases of coated inclusions, *International Journal of Solids and Structures* 43 (2006) 2513–2541.
[21] Y.M. Yi, S.H. Park, S.K. Youn, Asymptotic homogenization of viscoelastic composites with periodic microstructures, *International Journal of Solids and Structures* 35 (1998) 2039–2055.
[22] Y.M. Yi, S.H. Park, S.K. Youn, Design of microstructures of viscoelastic composites for optimal damping charateristics, *International Journal of Solids and Structures* 37 (2000) 4791–4810.
[23] E.M. Kerwin Jr., E.E. Ungar, Requirements imposed on polymeric materials by structural damping applications, in: R.D. Corsaro, L.H. Sperling (Eds.), *Sound and Vibration Damping with Polymers*, American Chemical Society, Washington, DC, 1990.
[24] M.A. Zocher, S.E. Groves, A three-dimensional finite element formulation for thermoviscoelastic orthotropic media, *International Journal for Numerical Methods in Engineering* 40 (1997) 2267–2288.
[25] M.W.D. Van der Burg, E. Van der Giessen, Delaunay-network modelling of creep failure in regular ploycrystalline aggregates by grain boundary cavitation, *International Journal of Damage Mechanics* 3 (1994) 111–139.
[26] L. Shuguang, On the unit cell for micromechanical analysis of fibre reinforced composites, *Proceedings: Mathematical, Physical and Engineering Sciences: Mathematical* 455 (1999) 815–838.
[27] O. Kristensson, N.J. Sorensen, B.S. Andersen, Concurrent finite element analysis of periodic boundary value problems, *Computer Methods in Applied Mechanics and Engineering* 192 (2003) 1877–1891.
[28] R.S. Lakes, High damping composite materials: effect of structural hierarchy, *Journal of Composite Materials* 36 (2002) 287–297.
[29] D. Gross, T. Seelig, *Fracture Mechanics: With a Introduction to Micromechanics*, Springer, Berlin, 2006.